2015

Hydrothermally-induced changes in mineralogy and magnetic properties of oxidized A-type granites

Lithos, v. 212/215, p. 145–157, 2015
http://www.producao.usp.br/handle/BDPI/48694

Lithos 212–215 (2015) 145–157

Contents lists available at ScienceDirect

Lithos

journal homepage: www.elsevier.com/locate/lithos

Hydrothermally-induced changes in mineralogy and magnetic properties of oxidized A-type granites

Anne Nédélec [a,*], Ricardo Trindade [b], Anne Peschler [a], Carlos Archanjo [c], Mélina Macouin [a], Franck Poitrasson [a], Jean-Luc Bouchez [a]

[a] UMR 5563, GET-OMP, Université de Toulouse, France
[b] Instituto de Astronomia, Geofísica e Ciências Atmosféricas, Universidade de São Paulo, São Paulo, Brazil
[c] Instituto de Geociências, Universidade de São Paulo, São Paulo, Brazil

ARTICLE INFO

Article history:
Received 24 April 2014
Accepted 4 November 2014
Available online 15 November 2014

Keywords:
A-type granites
Hydrothermalism
Magnetic susceptibility
Magnetite
Hematite
AMS fabrics

ABSTRACT

The changes in magnetic mineralogy due to the hydrothermal alteration of A-type granitic rocks have been thoroughly investigated in samples from the granite of Tana (Corsica, France), and compared with other A-type granites: Meruoca (NE Brazil), Bushveld (South Africa), Mount Scott (Wichita Mountains, Oklahoma, USA) and the stratoid hypersolvus granites of Madagascar. The altered red-colored samples and their non-altered equivalents were magnetically characterized by means of magnetic susceptibility measurements, hysteresis loops, remanent coercivity spectra, and Lowrie test. It is shown that hydrothermalization in magnetite-bearing granites is related to the formation of fine-grained magnetite and hematite, and to coeval depletion in the content of primary low-coercive coarse-grained magnetite. These mineralogical changes give typical rock magnetic signatures, namely lower susceptibility magnitudes and anisotropy degrees, prolate AMS (anisotropy of magnetic susceptibility) fabrics and increased coercivities. Optical microscopy and SEM (scanning electronic microscopy) images suggest that the orientation of the secondary magnetic minerals is related to fluid-pathways and micro-fractures formed during the hydrothermal event and therefore may be unrelated to magma emplacement and crystallization fabrics. Changes in magnetic mineralogy and grain-size distribution have also to be considered for any paleomagnetic and iron isotope studies in granites.

1. Introduction

A-type granitic rocks, as defined by Whalen et al. (1987), derive from hot magmas, which are able to ascend through the middle to upper crust without noticeable cooling. Due to decreasing pressure conditions, these water-undersaturated magmas become water-saturated and will release large amounts of water if they crystallize at shallow depths (Burnham, 1979). In the brittle crust, the exsolved magmatic fluids will encounter fractures, that may connect to the surface, hence the fluids will mix with surface-derived meteoritic or connate waters. The hydrothermal convective system thus created has major consequences on both the granitic rocks and their surroundings. Water–rock interactions are evidenced by mineralogical and chemical changes, collectively called hydrothermal alteration. For instance, biotite chloritization is a common piece of evidence for hydrothermal alteration in granitic rocks. In the field, hydrothermally-altered A-type granites are recognized by their pink to brick-red color, classically ascribed to the presence of tiny hematite inclusions in feldspars (Hofmeister and Rossman, 1983).

Hydrothermally-induced changes are controlled by a variety of parameters, such as temperature, oxygen fugacity, fluid composition and fluid/rock ratio. The nature of the fluids and the intensity of their action can be monitored by stable isotope studies (Marks et al., 2003; Rye, 1993). Hydrothermal processes are extensively studied for their contribution to the genesis of ore deposits. In addition, their influence on the granite accessory minerals that can suffer perturbation of their geochronological memory, such as zircon or monazite, was also accounted for by Poitrasson et al. (1998, 2000). The present work is aimed at presenting another effect of hydrothermal alteration, namely the main changes of the nature and content of iron-oxide accessories, using rock magnetic properties associated with microscopic observations. The study is focussed on the Tana granite from Corsica (France), but other granites of different ages, sizes, emplacement depths and hydrothermalization degrees are also used for comparison. For consistency, only magnetite-bearing (oxidized) A-type granites will be considered. These magnetite-bearing A-type granites form a well identified group (Anderson and Morrison, 2005). Changes in the magnetic properties will prove to be a very sensible indicator of interactions with fluids, even before the appearance of any mesoscopic feature of alteration.

* Corresponding author.
E-mail address: anne.nedelec@get.obs-mip.fr (A. Nédélec).

http://dx.doi.org/10.1016/j.lithos.2014.11.007
0024-4937/

2. Geological setting of the studied granites

Five A-type granites of various ages and sizes were selected for the study: the Tana granite (Corsica, France), the Meruoca granite (Brazil), the Bushveld granite (South Africa), the Mount Scott granite (Wichita Mountains, Oklahoma), and the alkaline stratoid granites of Madagascar. Their geological setting, petrography and mineralogy are described below. All these granites display a more or less pronounced hydrothermalization in relation with shallow to intermediate emplacement levels.

2.1. Tana granite (Corsica, France)

Located in south-western Corsica, the Tana granite is a small intrusion cropping out over 39 km^2. It is one of the A-type granitic complexes that were emplaced in Corsica during the waning stages of the Hercynian Orogeny. Bonin (1980, 1986) divided the Tana granite in three geographical units (Fig. 1a). The central part has an elliptic shape, that was suggested to be the roof of a ring-complex. The southern part of the Tana granite, called Punta di U Carbone, was emplaced as a wide NE-striking sheet along the small mafic layered intrusion of Peloso. The northern part, made of narrow dykes, will not be considered here.

The main rock type is an aluminous subsolvus biotite-bearing granite (Poitrasson et al., 1994). Bonin et al. (1987) obtained a Rb/Sr isochron age of 267 ± 6 Ma for the Tana granite. A more precise geochronological determination yielded 276 ± 3 Ma (2σ), although two samples from the Punta di U Carbone did not plot on the isochron (Poitrasson et al., 1994). However, these Rb–Sr ages have likely been rejuvenated by subsequent hydrothermal circulations since more recent U–Pb determinations on zircons led to older ages of 291.2 ± 2.6 Ma (2σ) by SHRIMP for the Punta di U Carbon intrusion and 292 ± 8 Ma by evaporation on the Tana granite main intrusion (Cocherie et al., 2005). In the central part, the granite is very heterogeneous in grain size and its color changes from whitish to pink. In the Punta di U Carbone, the granite is medium- to coarse-grained and displays a conspicuous brick-red color mainly due to the feldspar grains. The magma was emplaced at a shallow level, as witnessed by fined-grained to microlitic quenched borders. The primary mineral composition comprises quartz, perthitic alkali feldspar, plagioclase, biotite and accessories. Hydrothermalization appears to have occurred everywhere at various degrees. It is revealed by the replacement of primary phases

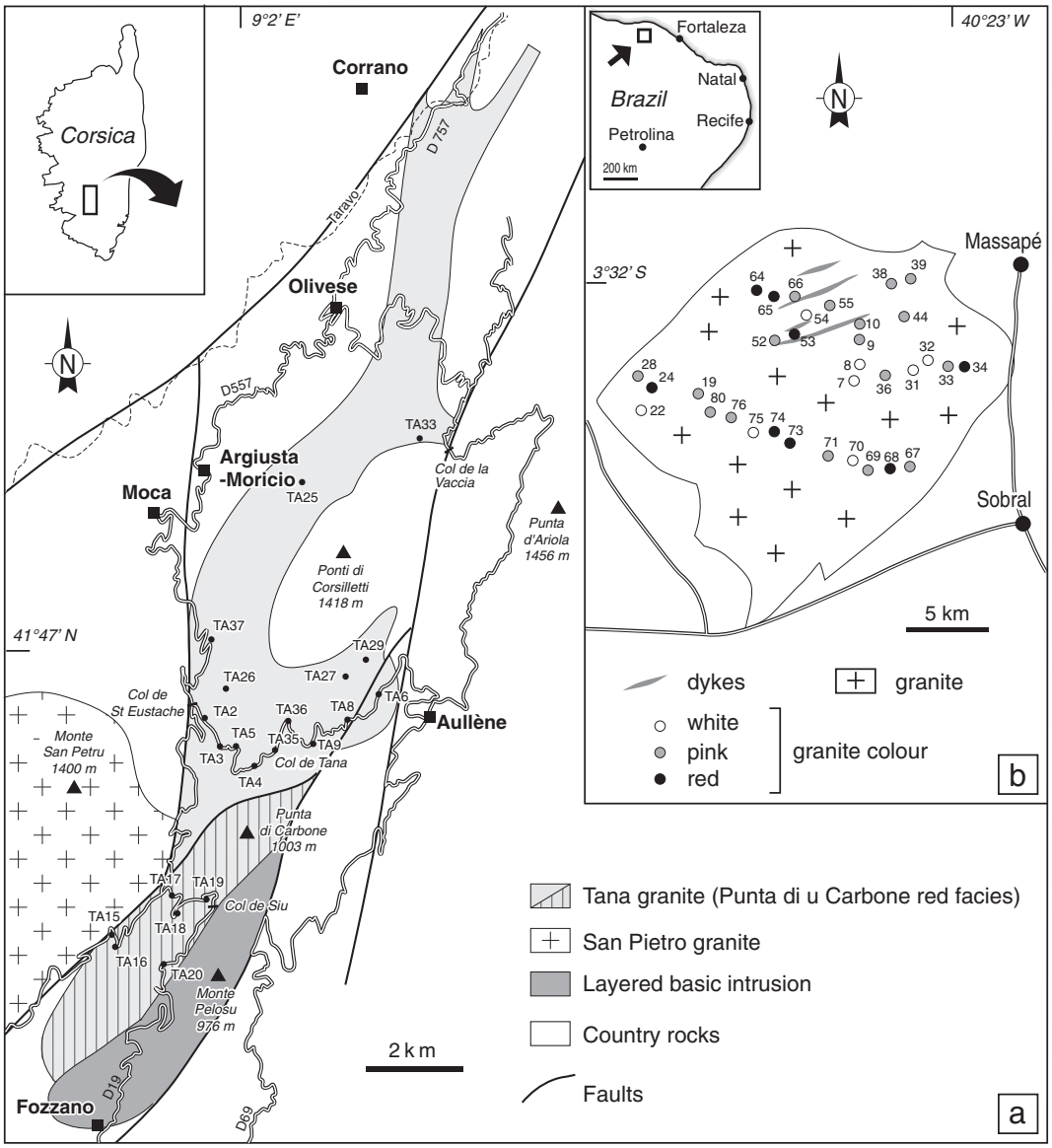

Fig. 1. Location of sampling sites in: (a). Tana pluton (Corsica) and (b) Meruoca pluton.

by secondary minerals and coincides with a reddish color in the most altered samples. Chlorite formed after biotite; it is associated with very small titaniferous phases and sometimes contains lamellar K-feldspar, pointing to chloritization in medium- to high-temperature conditions (Bailey, 1984). Magnetite is present either as small grains in biotite or as large grains with ilmenite–magnetite trellis exsolutions. Magnetite grains show peripheral oxidation to hematite in some samples.

2.2. Meruoca granite (Brazil)

The Meruoca pluton is one of the largest A-type late-Brasiliano intrusions emplaced at around 523 Ma in the Ceara Province of northeastern Brazil (Santos et al., 2008). According to Sial et al. (1981), this pluton is made of granites and quartz-syenites. Most rocks are pink to brick-red alkaline to peralkaline granitic rocks. A green to gray fayalite-bearing unit is restricted to the northern part of the pluton. The granites contain quartz, alkali-feldspar, plagioclase, alkali-calcic amphibole, biotite, magnetite and minor accessories. Some samples display granophyric textures indicative of shallow-depth emplacement. The common reddish colors and turbid feldspars point to a pervasive hydrothermal alteration. $\delta^{18}O$ data (Sial and Long, 1987) follow a concentric pattern inside the pluton and confirm low-temperature interaction with meteoritic waters. Major and trace element contents are typical of an A-type suite, with a dominantly peraluminous character. Samples from an E–W profile through the southern part of the pluton have been studied in detail for their magnetic properties (Fig. 1b).

2.3. Bushveld granite (South Africa)

The Bushveld Complex (Daly, 1928) is a huge bimodal intrusion, made of mafic layered series overlain by a granitic layer reaching 3 km in thickness and covering an area of about 66,000 km^2. Present exposure is but half due to both erosion and deposition of a younger sedimentary cover. Nevertheless, the Bushveld granite remains the largest intrusion of A-type granite in the world. It has been dated at 2055 ± 2 Ma by the Pb evaporation method on single zircons (Walraven and Hattingh, 1993). The entire granitic mass crystallized at a shallow level, i.e. at pressures between 100 and 200 MPa.

Two granitic lithologies are recognized and extensively described by Kleemann and Twist (1989). The main one is the coarse-grained hypersolvus Nebo Granite, that shows a vertical mineral zonation characterized by a decreasing hornblende content from bottom to top, as well as a gradual change in color from gray to red. Accessories are mainly zircon, allanite, ilmenite and magnetite. Opaque minerals crystallized rather early as subhedral grains, presently often included in the interstitial ferro-magnesian minerals. The Nebo Granite was emplaced as a water-undersaturated, hot, restite-free magma. Its initial water-content is estimated at around 2 wt.%. In situ fractional crystallization ended in a saturated residual liquid containing about 5 wt.% H_2O, leading to the separation of a discrete hydrous fluid phase that progressively concentrated towards the roof. The second granite type is the pink and fine-grained Klipkloof Granite that generally overlies and sometimes intrudes the Nebo Granite. This granite contains a high proportion of secondary and hydrothermal phases, but no magnetite. Robb et al. (2000) recognize three stages of hydrothermalization in the Bushveld granites. The early one is due to fluid saturation of the magma and is responsible for cassiterite mineralization and sericitization. Sulfides crystallize during the second stage, characterized by lower-temperature fluids of mixed magmatic and meteoric origin. The last stage occurs more than 50 Myr after granite crystallization and is characterized by sulfides and hematite precipitated along fractures by an external fluid.

Studied samples (kindly provided by R.G. Cawthorn) are sections of a vertical core extracted from the eastern limb of the Bushveld granitic layer (Fig. 2). The upper part of the core is reddish and coarse-grained; the lower part is light gray and coarse-grained. Hence, it appears that the core mainly sampled the Nebo granite with different degrees of hydrothermal alteration. Nevertheless, a 400 m-high section in the upper half of the core is made of a pink and finer-grained granite, that likely represents the Klipkloof granite type.

2.4. Mount Scott Granite (Wichita Mountains, USA)

Mount Scott Granite is the largest granitic sheet of the Wichita Granite Group that was emplaced in the Southern Oklahoma Aulacogen in relation to the Cambrian breakup of the Laurentian Supercontinent (Gilbert, 1983). It extends over 55 km in length and 17 km in width, but never exceeds 0.5 km in thickness. Mount Scott Granite is a typical A-type granite with a medium- to fine-grained hypersolvus texture (Hogan et al., 1992). Mafic minerals (amphibole, biotite and magnetite) represent less than 5% of the modal composition. The Mount Scott granite was emplaced at a very shallow depth corresponding to pressures as low as 50 MPa (Hogan and Gilbert, 1995). At the exposure level, it is characterized by a strong reddish color. Samples cored from a deeper level are pinkish gray. Two representative samples of each granite type were kindly provided by M.C. Gilbert.

2.5. A-type stratoid granites of Madagascar

The so-called stratoid granites of central Madagascar are shallowly-dipping sheet-like granites syntectonically emplaced at around 630 Ma (Paquette and Nédélec, 1998) into upper-amphibolite facies gneisses and migmatites. In contrast to the other plutonic complexes described above, the Madagascan sheets were emplaced at mid-crustal levels, i.e. at depths comprised between 10 and 15 km (Nédélec et al., 1994).

Two granitic suites were recognized by Nédélec et al. (1995). Only the strongly alkaline suite made of quartz-syenites and hypersolvus alkali feldspar granites is retained for the present study. The quartz-syenites are dark greenish rocks containing perthitic alkali feldspar, clinopyroxene, amphibole and magnetite as main minerals. The alkali feldspar granites are light gray to pink fine-grained rocks and contain quartz, perthitic alkali feldspar, calcic to sodi–calcic amphibole and magnetite. Despite their leucocratic nature, magnetite is always present in large amounts: the rocks are therefore typical oxidized A-type granites that crystallized at relatively high fO_2 conditions. Hydrothermal alteration is restricted to a few samples and most rocks appear unmodified in thin sections. Oxygen isotope data (Nédélec et al., 1995) show that the syenites and the hypersolvus granites belong to a low $\delta^{18}O$ suite characterized by values at around 6‰, typical of mantle-derived rocks (Sheppard, 1986). One sample of pink hypersolvus granite (MG 60) displays a value as high as 9.5‰, likely explained by late-interaction with low-temperature oxidizing fluids (Wenner and Taylor, 1976). It is worth to notice that not all pink granites are characterized by high $\delta^{18}O$ values.

3. Material and methods

For the Tana, Madagascar and Meruoca granites, measurements were performed in a wide collection of samples extracted at evenly spaced sites covering all the surface of the respective granite bodies. Sampling location for Tana (98 samples) and Meruoca (91 samples) are provided in Fig. 1a and b respectively. Location of the sampling sites for the 43 specimens of hypersolvus stratoid granites and syenites of Madagascar is given in Nédélec et al. (1994). For the Bushveld granite, the 15 studied specimens were redrilled from the vertical core and were numbered after their respective depths. At last, for the Wichita Mount Scott sill, only two representative specimens were considered, namely a red altered sample (Wa1) and a gray unaltered sample (Wa2).

Magnetic mineralogy was investigated through anisotropy of magnetic susceptibility (AMS) measurements, thermomagnetic profiles,

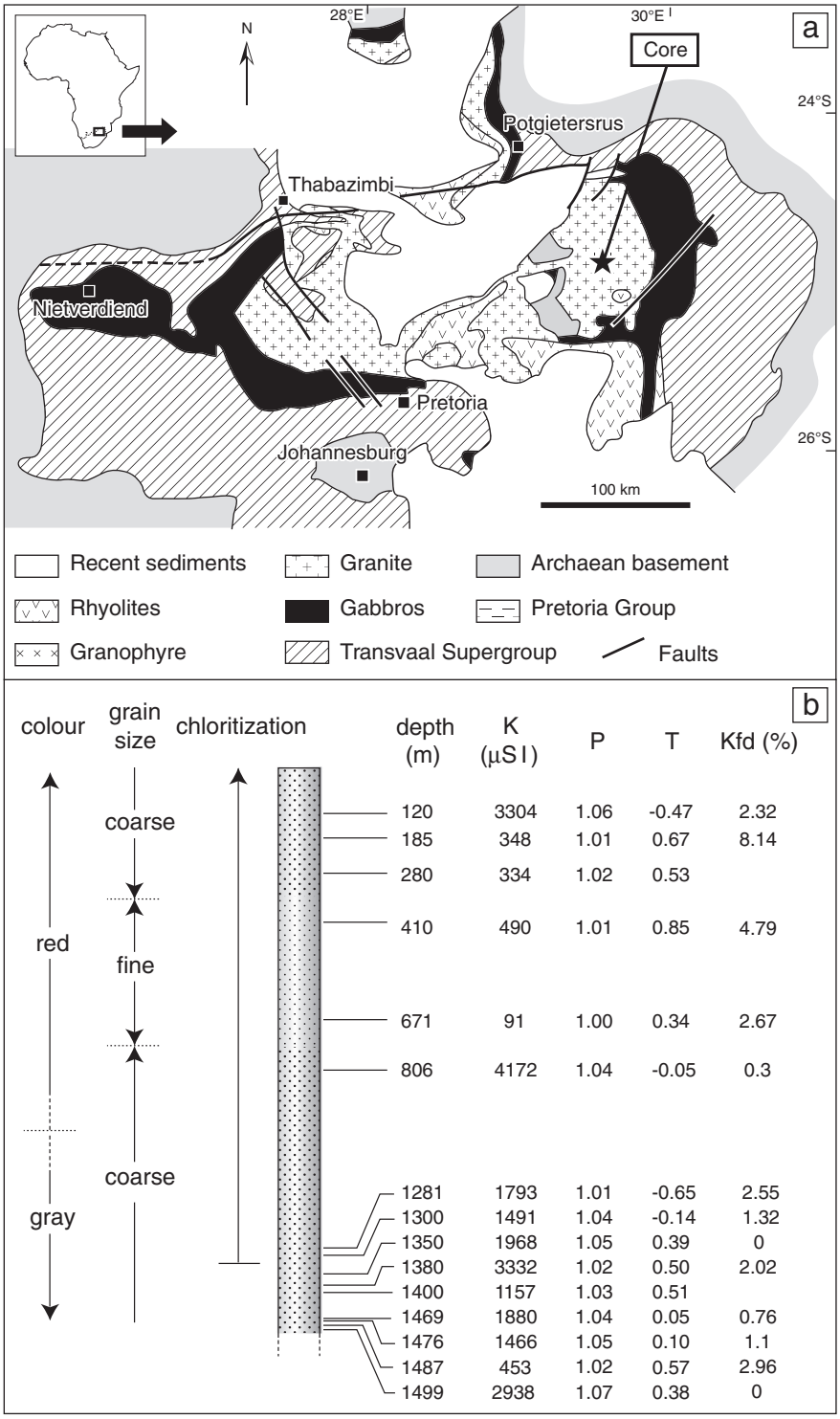

Fig. 2. The Bushveld granite core and relevant susceptibility data.

hysteresis loops, coercivity spectra, isothermal remanent magnetization (IRM) acquisition curves, and the Lowrie test (Lowrie, 1990).

Magnetic susceptibility and anisotropy were measured at low-field (3.8×10^{-4} T, 920 Hz) on a KLY2-bridge. Results are reported for individual samples, unlike classical studies, where averages of results for a variable (usually 3 to 6) number of samples are used for structural purpose. The frequency-dependent magnetic susceptibilities were measured in a Bartington susceptibility meter equipped with a MS2B dual-frequency sensor working at 0.47 and 4.7 kHz. Thermomagnetic curves were obtained using the same instrument coupled to a CS2/CSL furnace from −190 to 700 °C. Anhysteretic remanence, its anisotropy (AAR), and remanent coercivity spectra were obtained using a JR5A magnetometer (sensitivity of less than 100 A/m) and an LDA3-AMU1 magnetizer/demagnetizer (Agico). AAR measurements were performed for low-coercivity grains (between 0 and 20 mT) and for those with remanent coercivities comprised between 40 and 60 mT. Remanent coercivity spectra were determined from 0 up to 90 mT, at 10 mT intervals. IRM acquisition curves up to 3 T were performed on representative samples of the altered and non-altered facies. The same samples were further thermally demagnetized after IRM acquisition along three

Table 1
AMS data from Tana (Corsica). K: susceptibility magnitude; P: anisotropy degree; T: shape parameter; Kfd: frequency-dependent susceptibility.

Specimen	K (10^{-6}SI)	P = K1/K3	T	Kfd (%)
Tana (center)				
TA 2 A1	1780	1.09	−0.09	
TA 2 A2	1590	1.07	0.05	
TA 2 A3	1500	1.05	0.19	
TA 2 A4	1900	1.11	0.31	
TA 2 B1	1720	1.1	0.43	
TA 2 B2	1100	1.1	0.35	
TA 2 C1	1830	1.03	0.8	
TA 2 C2	2210	1.11	−0.13	
TA 3 A1	90	1.06	0.09	
TA 3 A2	70	1.08	0.27	
TA 3 B1	310	1.16	−0.08	
TA 3 B2	320	1.08	−0.54	
TA 3 C1	50	1.03	0.08	
TA 3 C2	180	1.17	−0.32	
TA 3 C3	150	1.03	−0.32	
TA 4 A1	90	1.03	0.35	
TA 4 A2	60	1.02	−0.05	
TA 4 A3	80	1.03	0.22	
TA 5 A1	540	1.08	−0.1	
TA 5 A2	390	1.05	−0.28	0.63
TA 5 A3	1440	1.05	0.51	0.99
TA 5 B1	680	1.09	−0.24	0
TA 5 B2	1130	1.08	−0.58	0.69
TA 5 C1	180	1.07	0.76	
TA 5 C2	490	1.05	−0.02	
TA 5 C3	720	1.06	−0.35	1.05
TA 6 A1	1090	1.09	−0.16	0
TA 6 A2	2720	1.13	0.35	0.2
TA 6 B1	2000	1.09	0.77	1.31
TA 6 B2	1400	1.09	0.63	1.28
TA 6 C1	1370	1.08	0.21	0.75
TA 8 A1	4520	1.04	−0.65	
TA 8 A2	2500	1.05	0.69	
TA 8 C1	70	1.03	0.61	
TA 9 A1	370	1.08	0.58	
TA 9 B1	30	1.01	−0.63	
TA 9 C1	30	1.02	−0.04	
TA 9 C2	20	1.01	0.13	
TA 9 D1	30	1.03	−0.22	
TA 25 A1	4520	1.17	−0.18	0.21
TA 25 A2	3770	1.15	−0.03	1.69
TA 25 B1	2870	1.14	−0.25	0.14
TA 25 B2	4000	1.18	0.53	0.04
TA 25 C1	4060	1.13	−0.08	0.63
TA 26 A11	4230	1.05	0.34	
TA 26 A21	30	1.01	0.01	
TA 26 B11	3140	1.06	0.14	
TA 26 B12	4670	1.06	−0.3	
TA 26 B21	30	1.01	0.46	
TA 27 A1	1880	1.03	−0.16	0.35
TA 27 B1	2340	1.14	−0.16	0.46
TA 27 B2	2170	1.11	0.07	
TA 27 C1	110	1.01	0.6	
TA 27 C2	110	1.02	−0.26	
TA 29 A1	380	1.08	0.2	0
TA 29 A2	320	1.04	0.31	
TA 29 B1	910	1.06	0.64	
TA 29 B2	920	1.16	−0.02	0.57
TA 29 C1	270	1.03	0.42	3.24
TA 29 C2	430	1.08	−0.23	1.18
TA 33 A1	1470	1.04	0.65	0.35
TA 33 B1	1920	1.05	0.6	0.19
TA 33 B2	2040	1.04	0.79	0
TA 35 B1	3900	1.04	−0.28	
TA 35 B2	6870	1.03	−0.45	
TA 36 A2	1490	1.07	0.69	
TA 36 A3	780	1.06	0.76	
TA 36 B1	1230	1.06	−0.33	
TA 36 C1	60	1.02	−0.3	
TA 36 C2	60	1.02	0.09	
TA 37 B1	900	1.1	−0.15	
TA 37 C1	180	1.06	0.53	
TA 37 C2	300	1.07	−0.13	0.41
TA 37 C3	330	1.06	0.39	
Punta di U Carbone				
TA 15 C1	3140	1.07	0.02	0.57
TA 15 D1	3410	1.04	0.17	0.47
TA 16 A1	1730	1.03	−0.33	
TA 16 B1	1160	1.04	0.56	
TA 16 B2	1380	1.05	0.5	
TA 16 C1	1280	1.06	0.17	
TA 16 C2	1540	1.03	−0.19	
TA 17 C1	760	1.02	0.57	0.98
TA 17 D1	730	1.02	−0.19	
TA 18 A1	630	1.04	−0.06	1.47
TA 18 B1	660	1.04	0.48	
TA 18 B2	680	1.04	0.47	
TA 18 C1	280	1.02	0.89	3.62
TA 18 C2	290	1.03	−0.16	
TA 19 A1	1720	1.04	−0.59	
TA 19 A2	400	1.03	−0.57	
TA 19 B1	1200	1.03	−0.22	
TA 19 B2	1120	1.03	0.44	
TA 19 C1	700	1.02	0.49	
TA 19 C2	420	1.03	0.03	
TA 20 A1	280	1.05	0.53	
TA 20 A2	340	1.03	0.43	
TA 20 B1	460	1.04	−0.41	
TA 20 B2	400	1.02	−0.24	
Average	1267	1.06	0.12	
Minimum	22	1.01	−0.59	
Maximum	6871	1.10	0.79	

orthogonal directions with different peak fields (3, 0.4 and 0.12 T) to estimate unblocking temperatures of the soft (<0.12 T), medium (0.12–0.4 T) and hard (>0.4 T) coercivity fractions. Hysteresis curves for Tana granite were obtained in the LSCE (Laboratoire des Sciences de l'Environnement et du Climat) by courtesy of C. Kissel. Other hysteresis data were acquired in São Paulo University.

For all the studied plutons, a series of polished thin sections was examined through optical and scanning electronic microscopy to determine the location of the different magnetic phases.

4. Magnetic fingerprints of hydrothermal changes

4.1. Magnetic susceptibility

4.1.1. Magnetic susceptibility magnitude

Lapointe et al. (1986), Harding et al. (1988) and Just et al. (2004) already noticed that alteration strongly lowers the magnetic susceptibility of plutonic rocks, as a consequence of a lowered magnetite content. Susceptibility magnitudes of the selected A-type granites are presented in Fig. 2 and Tables 1, 2 and 3. As a whole, they display a wide range of values. The values for the stratoid granites of Madagascar are one order of magnitude higher than in the other granites. However, averages for each granite are high enough to be consistent with the presence of magnetite in most samples, taking into account the susceptibility limit defined by Rochette et al. (1992). Indeed, these authors proposed that susceptibility magnitudes (K) lower than 500 μ SI characterize paramagnetic rocks devoid of any magnetite.

Three collections of data contain enough samples to enable a statistical analysis of the scalar susceptibility data, namely: the Tana granites, the hypersolvus stratoid granites (and quartz-syenites) of Madagascar and the Meruoca granites. Analysis of the distribution of the susceptibility magnitudes is presented as cumulative frequency curves on a logarithmic scale (Fig. 3). In such a representation, samples plotting on the same linear segment correspond to a unimodal susceptibility distribution likely related to magmatic differentiation (Lapointe et al., 1986). By contrast, recognition of two (or more) linear segments point either to the co-existence of different magmas or to some overprint by other processes, such as alteration after magmatic crystallization.

Table 2
AMS data from Meruoca (Brazil). K: susceptibility magnitude; P: anisotropy degree; T: shape parameter.

Specimen	K (10^{-6} SI)	P = K1/K3	T
Me7a1	1799	1.03	0.04
Me7a2	2990	1.01	0.63
Me7b1	970	1.03	0.08
Me7b2	1989	1.05	−0.36
Me8a1	1641	1.02	−0.40
Me8a2	1261	1.02	0.26
Me8b1	3307	1.03	−0.23
Me8b2	2280	1.03	0.52
Me9a1	1565	1.02	0.46
Me9a2	2413	1.04	−0.62
Me9b1	2526	1.04	0.08
Me9b2	2133	1.05	0.39
Me10a1	1163	1.01	0.18
Me10a2	898	1.01	0.10
Me10b1	1052	1.02	−0.52
Me10b2	1587	1.01	0.81
Me19a1	207	1.01	0.03
Me19a2	129	1.02	−0.06
Me19b1	152	1.02	−0.31
Me19b2	209	1.03	0.33
Me22a1	330	1.01	0.76
Me22a2	916	1.03	0.76
Me22b1	1323	1.04	0.50
Me22b2	1611	1.03	0.75
Me24a1	1834	1.02	−0.68
Me24a2	1916	1.01	0.12
Me24b1	353	1.01	−0.06
Me24b2	546	1.02	−0.40
Me20a1	1842	1.03	−0.24
Me20a2	2699	1.03	−0.61
Me20b1	1014	1.01	−0.15
Me20b2	825	1.03	0.06
Me31a1	2922	1.05	0.10
Me31a2	2345	1.04	−0.54
Me31b1	2183	1.04	−0.07
Me31b2	2053	1.03	0.76
Me32a1	2311	1.04	0.03
Me32a2	543	1.02	−0.22
Me32b1	603	1.06	0.02
Me32b2	2244	1.03	0.01
Me33a1	8317	1.03	0.08
Me33a2	11,910	1.03	−0.16
Me33b1	2262	1.03	0.53
Me33b2	5332	1.05	−0.34
Me34a1	1686	1.03	−0.47
Me34a2	2116	1.09	−0.11
Me34b1	8223	1.03	0.47
Me34b2	4008	1.07	0.47
Me36a1	860	1.05	0.10
Me36a2	2646	1.03	−0.10
Me36b1	755	1.02	−0.41
Me38a1	68	1.01	−0.51
Me38a2	79	1.01	0.50
Me38a3	65	1.02	0.30
Me38b2	74	1.01	0.03
Me38b3	71	1.02	0.87
Me39a1	2421	1.07	0.26
Me39a2	3157	1.12	0.06
Me39b1	2389	1.05	0.30
Me44a1	1351	1.04	0.50
Me44a2	2402	1.02	0.37
Me44b1	1038	1.04	−0.39
Me44b2	1787	1.03	−0.09
Me52a1	2377	1.06	−0.37
Me52a2	1988	1.03	0.19
Me52b1	1463	1.03	−0.16
Me52b2	1746	1.04	0.19
Me52c1	32,840	1.05	−0.68
Me52c2	19,450	1.05	0.59
Me53a1	1423	1.03	0.42
Me53a2	1846	1.01	−0.44
Me53b1	1400	1.02	0.88
Me53b2	1825	1.01	−0.33
Me54a1	3877	1.03	0.55
Me54a2	5032	1.02	0.46
Me54b1	4276	1.02	0.61
Me54b2	4829	1.03	0.60
Me55a1	2668	1.04	0.53
Me55a2	1683	1.04	0.30
Me55b1	3655	1.04	−0.17
Me55b2	2763	1.04	0.45
Me64a1	2143	1.04	0.89
Me64a2	1452	1.03	0.67
Me64b1	843	1.03	0.55
Me64b2	1132	1.04	0.45
Me65a1	902	1.03	−0.36
Me65a2	1212	1.06	0.21
Me65b1	680	1.09	0.07
Me65b2	1835	1.03	0.19
Me66a1	4518	1.02	0.68
Me66a2	3778	1.02	0.35
Me66b1	3324	1.03	0.03
Me66b2	6252	1.03	−0.12
Me67a1	1762	1.02	−0.05
Me67a2	1641	1.02	0.85
Me67b1	1211	1.01	−0.55
Me67b2	667	1.05	−0.24
Me68a1	905	1.03	0.09
Me68a2	1119	1.03	−0.45
Me68b1	5573	1.02	0.17
Me68b2	3186	1.03	0.08
Me69a1	1507	1.06	0.32
Me69a2	1835	1.04	0.61
Me69b1	4194	1.02	−0.44
Me69b2	2794	1.02	−0.01
Me70a1	1130	1.02	−0.25
Me70a2	1723	1.03	−0.69
Me70b1	3809	1.02	0.07
Me71a1	2296	1.03	−0.00
Me71a2	1435	1.02	0.65
Me71b1	571	1.02	−0.35
Me71b2	636	1.04	−0.37
Me73a1	1533	1.03	−0.59
Me73a2	1966	1.03	0.10
Me73b1	2126	1.03	0.54
Me73b2	1972	1.04	0.36
Me74a1	4018	1.02	−0.83
Me74a2	2364	1.03	−0.18
Me74b1	2366	1.03	0.32
Me74b2	2918	1.02	0.47
Me75a1	1904	1.02	−0.56
Me75a2	1660	1.02	−0.15
Me75b1	5167	1.02	0.52
Me75b2	2314	1.02	−0.27
Me76a1	6041	1.03	0.40
Me76a2	5723	1.04	0.27
Me76b1	4337	1.05	−0.20
Me76b2	1690	1.03	0.38
Me80a1	117	1.01	0.73
Me80a2	97	1.02	0.55
Me80b1	149	1.01	0.26
Me80b2	140	1.01	−0.21
Me80b3	152	1.02	0.34

The three studied granites display at least two populations, but the susceptibility magnitudes separating these populations are different for each granite (Fig. 3). Two populations are recognized among the samples from Tana granite as a whole (Fig. 3a). The main population represents 80% of the samples with K ranging from 250 to 3500 μ SI. The 20% remaining samples have susceptibility magnitudes lower than 250 μ SI. Actually, these two populations characterize the central part of the Tana massif, representing respectively 70 and 30% of the samples. The southern Punta di U Carbone samples represent a homogeneous set with susceptibility magnitudes higher than 250 μ SI, undistinguishable from the rest of the main population regarding the distribution of K values, despite its specific brick-red color.

Table 3
AMS data from the hypersolvus stratoid granites of Madagascar. K: susceptibility magnitude; P: anisotropy degree; T: shape parameter.

Specimen	K (10^{-6} SI)	P = K1/K3	T
Granites			
MG 36 A1	11,960	1.54	0.39
MG 36 A2	6310	1.47	0.68
MG 36 B1	12,880	1.53	0.68
MG 36 B2	12,830	1.53	0.63
MG 94 A1	1080	1.26	0.28
MG 94 A2	1930	1.36	0.51
MG 94 B1	6790	1.59	0.04
MG 94 B2	45,380	1.81	0.43
MG 60 A1	1170	1.05	−0.09
MG 60 A2	2040	1.08	−0.03
MG 60 B1	2070	1.08	0.02
MG 60 B2	5620	1.18	0.16
MG 74 A1	18,090	1.51	0.7
MG 74 A2	20,560	1.5	0.85
MG 74 B1	13,400	1.34	0.79
MG 74 B2	16,410	1.47	0.7
MG 64 A1	31,580	1.67	0.52
MG 64 A2	23,930	1.67	0.39
MG 64 B1	20,720	1.56	0.3
MG 64 B2	22,990	1.59	0.52
MG 64 C1	300	1.06	−0.13
MG 64 C2	270	1.06	0.08
MG 9 A1	36,210	1.55	0.79
MG 9 A2	36,150	1.56	0.65
MG 9 B1	26,070	1.37	0.81
MG 9 B2	27,860	1.37	0.79
MG 14 A1	4050	1.31	0.48
MG 14 A2	4500	1.29	0.71
MG 14 B1	18,320	1.87	0.47
MG 14 B2	13,930	1.74	0.39
MG 100 A1	27,450	1.57	0.34
MG 100 A2	25,780	1.5	0.31
MG 100 B1	12,070	1.33	0.54
Quartz-syenites			
MG 91 A1	64,870	1.56	0.54
MG 91 A2	63,580	1.57	0.51
MG 91 B1	66,750	1.49	0.64
MG 91 B2	63,700	1.5	0.5
MG 72 A1	32,800	1.67	0.34
MG 72 A2	47,530	1.63	0.34
MG 72 B1	37,360	1.55	0.42
MG 93 A1	48,990	1.43	0.73
MG 93 A2	65,410	1.37	0.33
MG 93 A3	58,610	1.42	0.47
Averages	24,658	1.45	0.45
Min	270	1.05	−0.13
Max	66,750	1.87	0.85

The main population of Madagascan granites is characterized by K higher than 10,000 μ SI; lower K values characterize a second minor population representing about 30% of the samples (Fig. 3b). It is worth noticing that the samples where fluid–rock interactions were evidenced by additional chemical data (oxygen isotope or trace element data) belong to this second population. However, not all of them display a pink color.

The Meruoca granite also displays at least two different populations (Fig. 3c). The main population represents about 75% of the samples with susceptibility magnitudes between 1000 and 8000 μ SI. The second population amounts to about 20% of the samples with K less than 1000 μ SI. A few remaining samples with susceptibility magnitudes higher than 8000 and up to 15,662 μ SI (sample ME 52), likely belong to a third population. Reddish samples are observed in all three populations.

Samples from the Bushveld core (Fig. 2) form two subsets in relation to their depth: samples shallower than 700 m have susceptibility magnitudes less than 500 μ SI, whereas deeper samples (with one exception) display susceptibility magnitudes higher than 1000 μ SI. These two subsets correlate well with the bimodal distribution obtained by Ferré et al. (1999) from a larger database. In the area corresponding to the drilling site, Ferré et al. (1999) propose that K values lower than 750 μ SI correspond to hydrothermally altered rocks. Actually, biotite chloritization is observed in samples with higher susceptibility magnitudes (Fig. 2). Therefore, although low susceptibility samples were surely modified by hydrothermal processes, the very beginning of hydrothermal alteration cannot not be traced using this sole criteria.

A complete susceptibility log for an 87.5 m long core in the Mount Scott granite is given by Price et al. (1998). The grayish deeper part of the core corresponds to a magnetic susceptibility of ca 23,400 μ SI. Color changes to reddish orange from −30 m to the surface and, in the same time, the magnetic susceptibility decreases by two orders of magnitude.

4.1.2. Anisotropy degree

The anisotropy degree P is the ratio of maximum versus minimum susceptibility magnitudes (K1/K3). The range of values for the selected granites is given in Table 1. Once again, the alkaline stratoid granites of Madagascar differ from the other granites by a higher mean anisotropy degree of 1.45 and a wider range of values (1.05–1.87). These values are among the highest values encountered in ferromagnetic plutonic rocks (see Bouchez, 2000, for comparison). In these syntectonically emplaced magmas, Grégoire et al. (1998) established that such values reflect high shape ratios of primary magnetite grains. By contrast, the Meruoca and Bushveld granites display low anisotropy degrees, consistent with their emplacement as nearly undeformed shallow intrusions.

Variations of the anisotropy degree are analyzed in P vs. K diagrams (Fig. 4) with respect to the different populations of susceptibility magnitudes recognized above. In the Tana granite, samples from the southern Punta di U Carbone display a small range of values in-between 1.02 and 1.07 (Fig. 4a), whereas samples from the central part of the massif have a wider range of anisotropy values in-between 1.01 and 1.18 with a rough positive correlation with log K. The anisotropy degree of the main population of the stratoid granites is higher than 1.35, whereas the anisotropy degree of the second population (K < 10,000 μ SI) is lower than 1.60. Moreover, this latter population displays a rough positive correlation of P and K, especially clear in samples from sites (MG 60 and MG 64) that experienced fluid–rock interaction after geochemical data (Fig. 4b). No such correlation exists in the main population.

In the case of the Meruoca granite, the population having low susceptibility magnitudes also display very low anisotropy degrees (ca 1.02 in average), noticeably lesser than the remaining samples.

4.1.3. Shape parameter

The T parameter of Jelinek (1981) calculated as:

$$T = [2(\ln K2 - \ln K3)/(\ln K1 - \ln K3)] - 1$$

quantifies the shape of the AMS ellipsoid. Most granitic rocks are characterized by positive T values in agreement with their dominantly oblate magnetic fabric. Fig. 5 displays the T vs log K diagrams for Tana, Meruoca and Madagascar granites. Whereas most Madagascan granites plot in the positive T field, almost one third of the other granite samples plot in the negative field, pointing to a corresponding oblate magnetic fabric.

4.1.4. Frequency-dependent susceptibility

The frequency-dependent magnetic susceptibility is expressed as a percentage by

$$Kfd\,(\%) = 100\,[(Khf - Klf)/Klf]$$

where Khf and Klf are the magnetic susceptibilities respectively measured at high- and low-frequency (Dearing et al., 1996). It is an easy method to identify the presence of superparamagnetic (SP) magnetite grains, that correspond to very small grain sizes (<0.02 μm), sometimes abundant in soils and sediments (Font et al., 2006; Jackson et al., 1993; Maher, 1988). The specimens from the Bushveld core and a selection of specimens from Tana were selected for measurements and the results

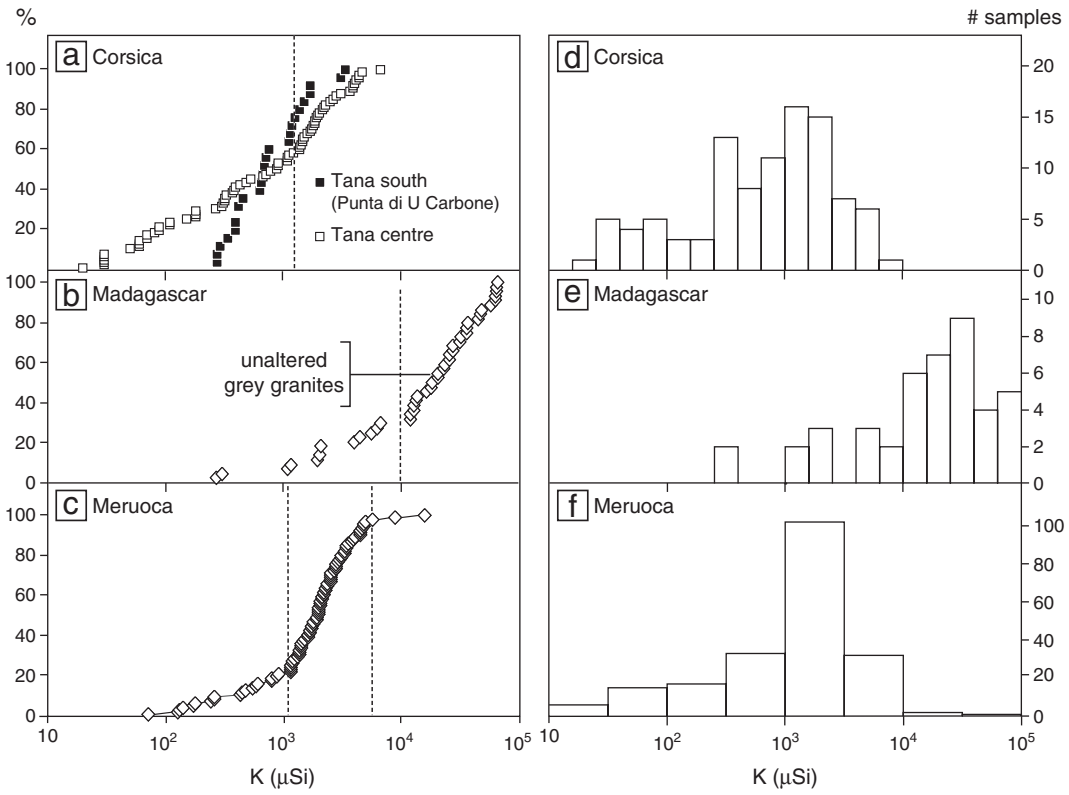

Fig. 3. Distribution of susceptibility magnitudes: (a) Tana; (b) stratoid granites of Madagascar; and (c) Meruoca.

are presented respectively in Fig. 2 and Table 1. There is a rough tendency for increased frequency-dependent susceptibility towards the surface in the Bushveld core and at least one sample (Kfd = 8%) displays a significant contribution of superfine grains. Conversely, the studied specimens of Tana granite display no or a small contribution of superfine particles without any peculiar spatial distribution.

4.2. Magnetic remanence and magnetic mineral carriers

4.2.1. Hysteresis parameters and remanent coercivity spectra

Hysteresis loops were performed for thirty samples from the Tana granite, comprising altered and non-altered rock-types. The shapes of the loops (Fig. 6a) correspond either to MD behavior in non-hydrothermalized granites or to wasp-waisted loops in hydrothermalized granites; this latter type of loop is typical of a mixture of magnetic grains (2 mineral phases or 2 grain-size populations of the same phase). In Day's diagram (Day et al., 1977, revised by Dunlop, 2002), the different rock-types plot into two distinct groups. Assuming that magnetite is present in all cases, Day's diagram enables a size-dependent interpretation of hysteresis properties for Bushveld, Tana, Mount Scott and Meruoca granites. Hydrothermalized granites usually show anomalously high hysteresis ratios, and plot very often in the pseudo-single domain field of the diagram (Fig. 6b). In contrast, non-altered granites are characterized by the predominance of a multi-domain behavior. The new curves relating the hysteresis parameters for different grain sizes of magnetite and their mixtures of Dunlop (2002) enable the refining of this conclusion. The hydrothermalized Tana, Mount Scott and Bushveld granites plot close to the mixing curve of SD and MD grains of pure magnetite. The Meruoca samples plot slightly off this line to the right.

The remanent coercivity spectra (RCS) acquired for the Tana and Wachita cases also reveal that major differences exist between altered and non-altered specimens (Fig. 7). The non-altered specimens have low-coercivity patterns typical of MD (multi-domain) magnetite. By contrast, significant shifts to high coercivity values are noticed in the altered specimens Ta18, Ta20 and Wa1 (Trindade et al., 2001). These differences in remanent coercivity distributions are attributed to changes in grain-size distributions of magnetite (Jackson et al., 1988), suggesting that these specimens contain a higher proportion of fine-grained particles.

4.2.2. Isothermal remanent magnetization (IRM) acquisition curves

The IRM acquisition curves for the different facies of the Meruoca granite are given in Archanjo et al. (2009). The greenish granite can be saturated at fields lower than 130 mT, hence only a soft (low coercivity) component is present. By contrast, some reddish granite samples are not saturated at 2.5 T, pointing to the existence of a second hard component. The IRM-acquisition curve for the hydrothermalized Tana granite also corresponds to two different (soft and hard) components, that can be identified using the fitting method of Kruiver et al. (2001). The presence of hematite, the high coercivity component, can be recognized by the bi-modal aspect of the GAP curve (the gradient of IRM acquisition curve) as well as the standardized acquisition plot (using a probability scale), as can be seen in Fig. 8.

4.2.3. Thermomagnetic curves and Lowrie test

Thermomagnetic curves presented by Ferré et al. (1999) for a few Bushveld specimens enabled discriminating the magnetite-rich unaltered granite (with a clear susceptibility drop at 580 °C and reversible heating and cooling curves) from hydrothermalized specimens with an ill-defined susceptibility drop and an increased susceptibility after heating, likely due to the formation of new magnetite from maghemite or hematite. However, none of the experiments yielded a Curie temperature typical of the presence of hematite. Indeed, small contents of hematite may not be evidenced by this method, because this mineral has a much lower susceptibility than magnetite. Changes in susceptibility magnitude with an increasing temperature (−190 °C to 700 °C) for the reddish Meruoca granite display a distinct drop at 580 °C, evidencing the presence of pure magnetite as the main magnetic carrier (Archanjo et al., 2009). A final small drop just before 700 °C is

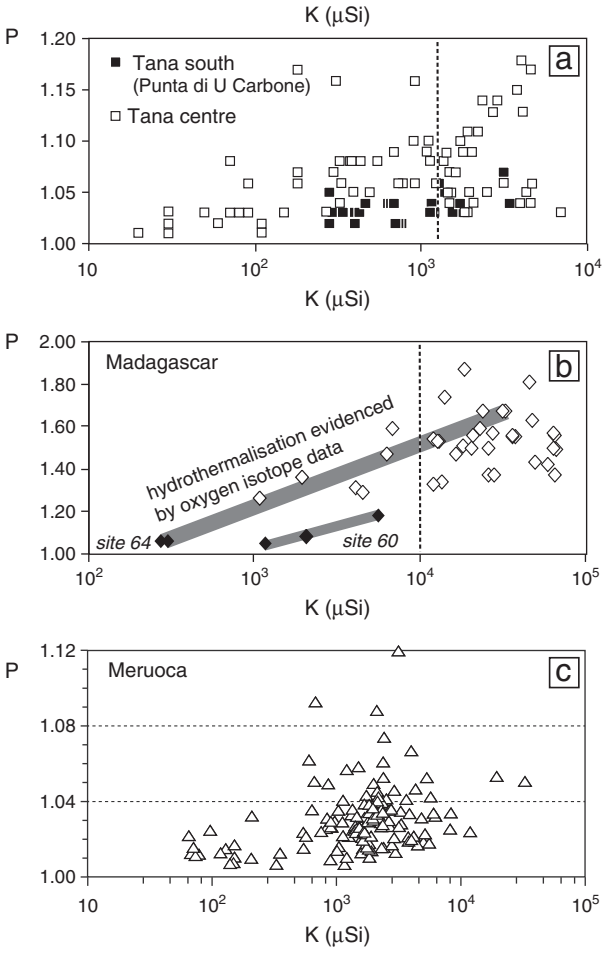

Fig. 4. P vs K: (a) Tana; (b) stratoid granites of Madagascar and (c) Meruoca.

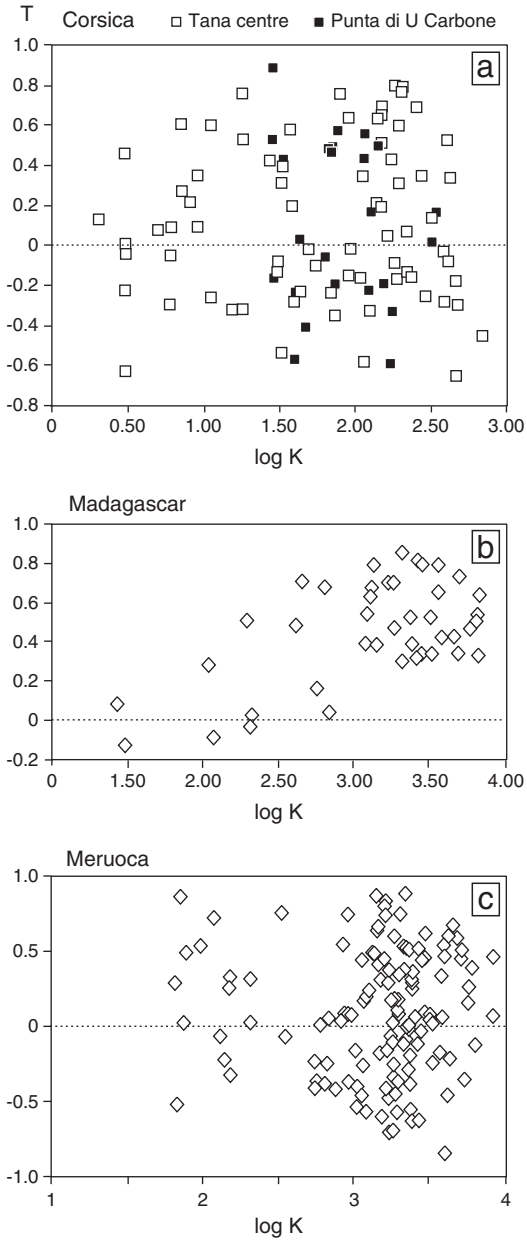

Fig. 5. T vs Log K: (a) Tana; (b) stratoid granites of Madagascar and (c) Meruoca.

often observed in these Meruoca specimens, evidencing the presence of hematite.

Changes in susceptibility magnitude on heating of two specimens (altered: Ta20, and non-altered: Ta8) of Tana granite were not able to evidence hematite (Fig. 9a). Both specimens present a similar pattern, with inflections around −150 °C (Verwey transition) and around 580 °C typically due to Ti-poor to pure magnetite, although their bulk magnetic susceptibilities at room temperature differ by one order of magnitude. No inflections around −15 °C and 675 °C, that would be related to hematite, are observed in these curves. However, the altered sample yields a hard remanence, not removed after AF demagnetization up to 100 mT, a feature attributed to a small fraction of hematite, a mineral indeed identified by microscopic studies and microprobe analysis (see below). Therefore, in order to prove the presence of hematite, the Ta19 sample was submitted to the Lowrie test (Lowrie, 1990). The sample is remagnetized in successively smaller fields along orthogonal directions and then thermally demagnetized. Results for each orthogonal component is plotted separately in Fig. 9b. The component with the highest remanent coercivity is demagnetized only at about 650 °C, close to the Curie temperature of hematite. However, this component contributes only for about 10% of the total remanence.

5. Microscopic study

All studied granites display primary (magmatic) grains of Fe(-Ti) oxides in thin sections. Their textural relationships point either to an early crystallization, as in the stratoid granites of Madagascar (Nédélec et al., 1995), or to a later, but still magmatic, formation as in the Bushveld granite (Ferré et al., 1999). Large primary grains of iron oxides obviously of magmatic origin were recognized in the Meruoca granite; they display typical magnetite–ilmenite exsolution features (Fig. 10a). In the altered Meruoca samples, the same oxide grains display more or less pronounced resorption of the magnetite-rich domains, whereas the ilmenite-rich exsolutions remain free of any alteration (Fig. 10b). Another generation of smaller oxide grains is associated to tiny fractures (Fig. 10c). Archanjo et al. (2009) also identified titanohematite with Ti-poor and Ti-rich exsolutions as small grains in chloritized biotite.

In the gray unaltered Wachita granite, iron oxides are observed as small inclusions in perthitic alkali feldspar (Fig. 10d). Microprobe analyses, sum of cations and calculation of structural formulae evidence that the larger inclusions (50 μm) are made of titanomagnetite and the smaller inclusions (10 μm) are actually made of titanohematite. Very similar Ti and Mn contents in all grains point to an origin of hematite by oxidation of former magnetite. According to the compositions, magnetite is likely of magmatic origin and the change of magnetite to hematite may be due to O-atom diffusion possibly due to some oxygen fugacity change in the magma, without any influence of a hydrous fluid phase as their alkali feldspar host is unaltered. By contrast, in the

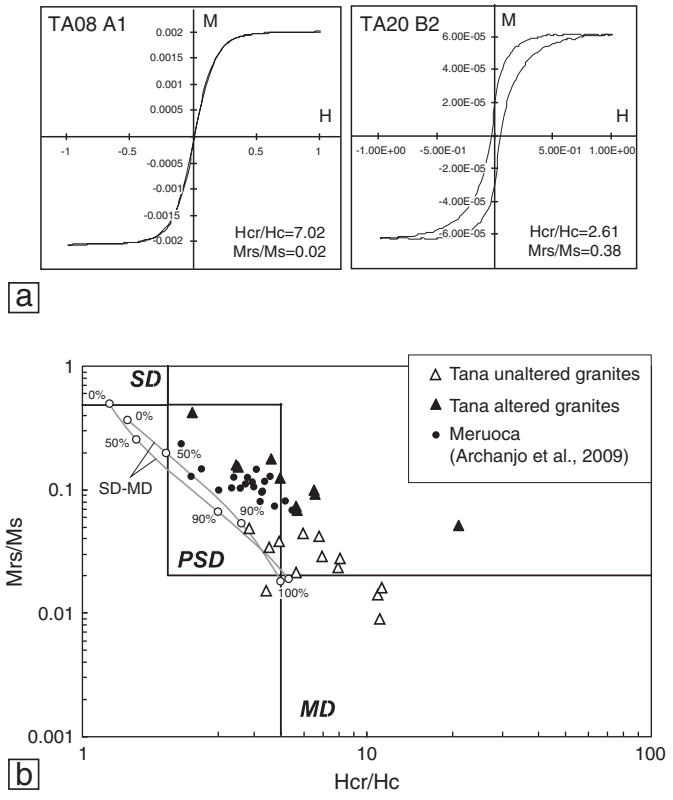

Fig. 6. Hysteresis curves for two Tana samples and plots of Tana and Meruoca in the Day diagram revised by Dunlop (2002).

hydrothermalized Tana granite, scanning electron microscope images show that tiny (5–15 μm) hematite crystals appear to have crystallized in vugs in the alkali feldspar grains (Fig. 10e) and are therefore surely related to water–rock interactions, as discussed by Putnis et al. (2007) for other reddish granites. At last, the brick-red color of the altered Wachita sample is due to a high content of hematite and/or iron hydroxides, either inside the grains, or in microfractures or as grain coatings likely due to surficial weathering (Fig. 10f).

6. Discussion and conclusions

6.1. Changes in magnetic properties and magnetic mineralogy

Hydrothermal alteration of magnetite-bearing A-type granites is responsible for lowering of the magnetic susceptibility magnitudes due to a decrease in magnetite contents. Hysteresis parameters generally follow a linear trend straddling the so-called PSD domain in the Day diagram, actually corresponding to a mixture of MD and SD magnetite grains. The proportions of SD grains is observed to be higher in the altered than in the unaltered samples. Hence, hydrothermal alteration is responsible for the dissolution of some of the primary MD magnetites associated to the crystallization of secondary SD grains. Besides, the formation of superfine (SP) particles seems not to be significant, with the exception of some very shallow Bushveld granite. Such SP Fe-oxides are regarded as the consequence of surficial weathering (Dideriksen et al., 2010). Fe-oxides of deeper origin, either hydrothermal or due to a late-magmatic oxidizing event, had time to grow to SD sizes or larger.

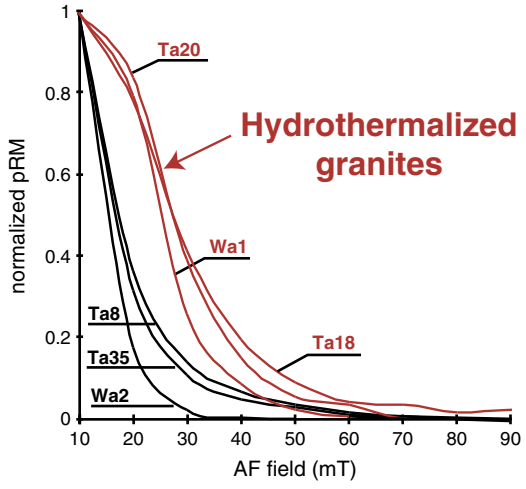

Fig. 7. Coercivity spectra of Tana and Wachita samples.

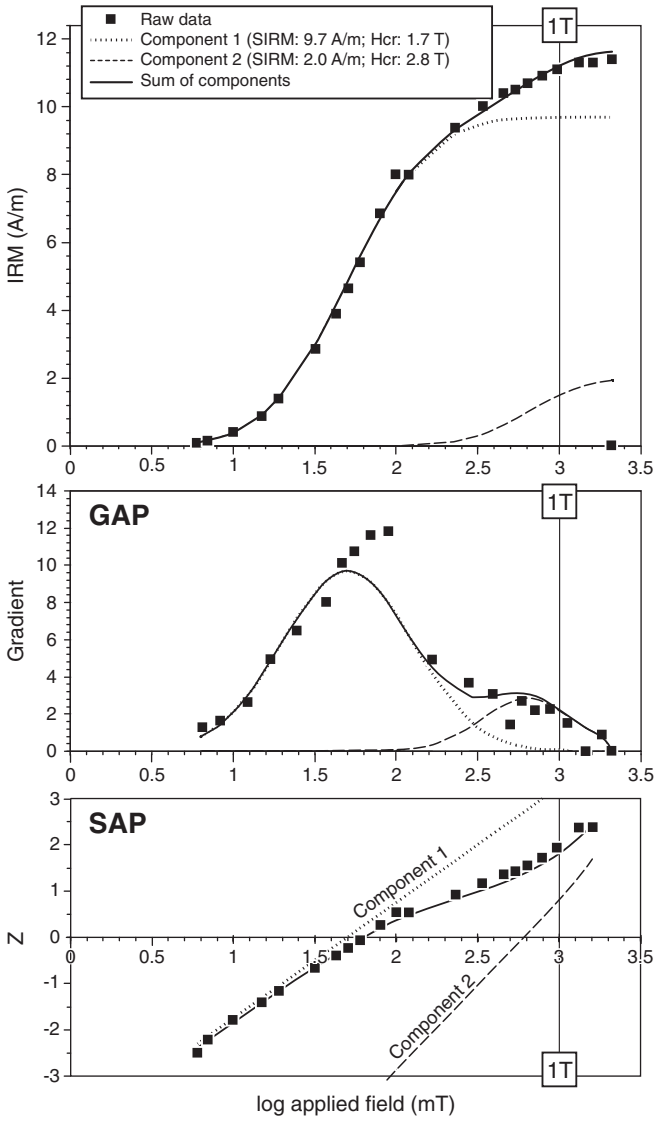

Fig. 8. IRM curve.

Modification of the magnetite grain-size distribution has an important consequence on the remanence properties of the altered rocks. The remanent coercivity spectra are consistent with the development of a hard coercivity component in the hydrothermalized granites, that could be either SD magnetite or hematite. The IRM acquisition curves confirm this interpretation. The thermomagnetic curves and especially the Lowrie test are the best means to identify hematite. The formation of hematite is generally related to fluid–rock interaction. Hematite appears in the hydrothermalized rocks even before these rocks acquire a pronounced reddish color. Actually, the change in color only appears when there is enough hematite and/or iron hydroxides. The first

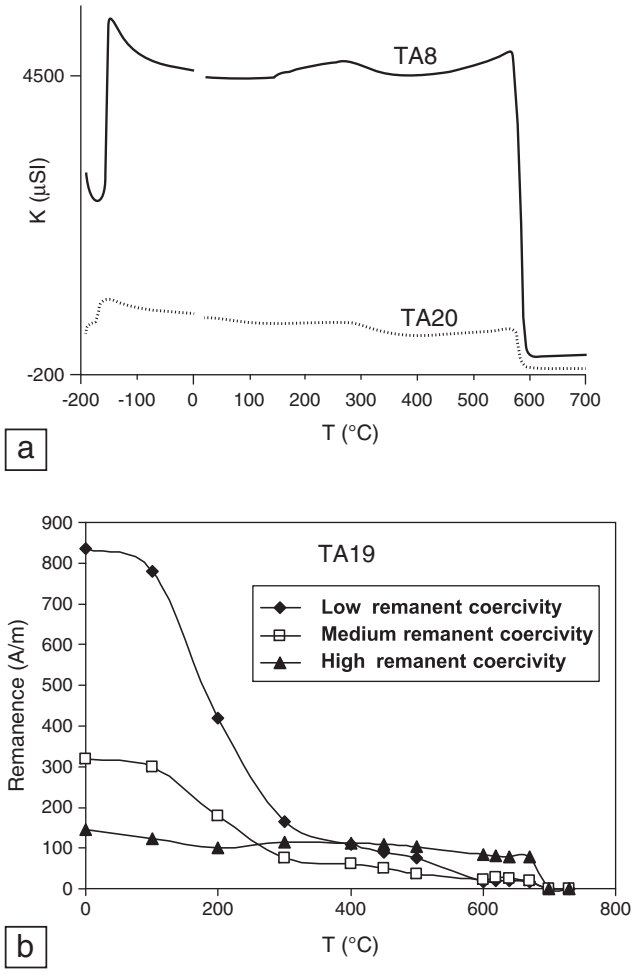

Fig. 9. (a) Thermomagnetic curves for two Tana samples. (b) Lowrie test curves (specimen Ta19 from Tana, Corsica).

appearance of hematite may sometimes occur before any substantial decrease of the magnetic susceptibility.

6.2. Implications for fabric analyses

The decrease in magnetic susceptibility associated to hydrothermal alteration also corresponds to a decrease in the anisotropy degree and, especially, to a change in the shape of the AMS ellipsoid as evidenced by an increasing number of negative values of the T parameter. These negative values correspond to an oblate AMS ellipsoid that reflect the shape fabric and/or distribution anisotropy of the magnetic mineral carriers. Since granite plutons are generally characterized by oblate magnetic fabrics, the few cases of prolate fabrics retained some attention, but received different interpretations. For instance, Riller et al. (1996) proposed that prolate susceptibility ellipsoids in the Murray pluton derive from the superposition of two (sub-)fabrics corresponding to different deformation events. Zák et al. (2005) interpreted prolate ellipsoids and the weak anisotropies in the core of the Sázava pluton as a preserved early magmatic fabric. In the present case studies, no superposed deformations have been evidenced. Moreover, it is impossible to consider the fabrics of hydrothermalized granites as early fabrics. Hence none of the previous interpretations can be retained.

The question arises of the coaxiality of the prolate fabrics of hydrothermalized granites with an earlier magmatic fabric. It is possible to answer comparing partial anhysteretic remanence anisotropy (pAAR) data acquired at field interval appropriate to separate the coarse-grained (low coercivity) magnetite fabric and the fine-grained (high coercivity) magnetite fabric. Indeed, this approach was already attempted by Trindade et al. (2001) for Ta20 and Wa1 specimens with contrasting results. The Tana specimen yields coaxial fabrics, whereas the Wachita specimen yields orthogonal fabrics. Indeed, the effect of the hydrothermal fluid was likely coeval with the emplacement of the Punta di U Carbone granitic magma as a single event. In many other cases, the fluid phase, either of magmatic or external origin, leaves its imprint after magma emplacement and just before or after full crystallization. In this case, the fine-grained fabric is acquired during hydrothermal alteration and mimics the fluid pathways, either channelized along foliation planes or along microfractures orthogonal to the foliation planes. Comparison of the AMS fabric with the mineral fabric acquired by an independent method may be also worth considering. This comparison has been attempted by Archanjo et al. (2009) for the Meruoca pluton, where mafic minerals define a subhorizontal magmatic foliation, while AMS of the reddish units show considerable scattering. Conversely, for the non-altered green to gray granites they found a good correspondence between magnetic and magmatic foliations. The interpretation is that the magnetic fabric of the hydrothermalized samples records (re)crystallization of iron oxides during secondary processes.

6.3. Perspectives

Hydrothermal alteration is generally responsible for the weakening of the magmatic fabric and for the possible acquisition of a secondary fabric. In this case, AMS-based structural studies have to be undertaken with caution. However, development of fine-grained magnetite and hematite in granites may be of great interest for paleomagnetic studies, because of the highly coercive nature of these minerals, provided that the hydrothermal event can be dated. Finally, the magnetic properties can offer a quick semi-quantitative estimate of fluid–rock interactions and may be of invaluable importance in the interpretation of stable isotopic data. Whereas modification of oxygen and hydrogen isotope signatures by fluid–rock interaction is already well known (e.g., Taylor, 1978), the discovery of heavy iron isotope signatures in some highly silicic A-types granites (Poitrasson and Freydier, 2005) is still a matter of debate. There are currently four hypotheses to account for this observation: 1) it may result from the exsolution of reduced fluids releasing isotopically light iron (Heimann et al., 2008; Poitrasson and Freydier, 2005; Telus et al., 2012). 2) This could be due to the fractional crystallization of specific oxides towards the end of the magma evolution (Schoenberg and von Blanckenburg, 2006; Schuessler et al., 2009; Sossi et al., 2012). 3) This may trace thermodiffusion in the silicic melts (Huang et al., 2010; Lundstrom, 2009). 4) More recently, a polymerization mechanism at the end of the magma evolution has been put forward (Dauphas et al., 2014). However, those mechanisms are not mutually exclusive and they may occur depending on the type of magmatism (Telus et al., 2012). Weathering may eventually complicate the message (Saunier et al., 2010; Wiederhold et al., 2007). It is thus suggested that future iron isotope studies in granites may benefit from concomitant magnetic studies as an efficient way to unravel the respective influence of magmatic, hydrothermal and supergene processes.

Acknowledgements

Technical assistance by Pierre Lespinasse, Christiane Cavaré-Hester, Anne-Marie Roquet and Philippe de Parseval from the GET (formerly LMTG) laboratory is greatly acknowledged. Special thanks are directed to Catherine Kissel for the use of the VSM instrument by A. Peschler in the LSCE laboratory (Gif-sur-Yvette) and to Irene Raposo for the use of the Kappabridge instrument by C. Archanjo in the Geociências laboratory (Sao Paulo). Financial support by the INSU-3F (*Failles*, *fractures*, *flux*) 2008 project of A. Nédélec was welcome, as well as the MAE contribution for R. Trindade staying in Toulouse. We appreciate the contribution of the two reviewers, M. Jackson and P. Camps, that significantly improved the original manuscript.

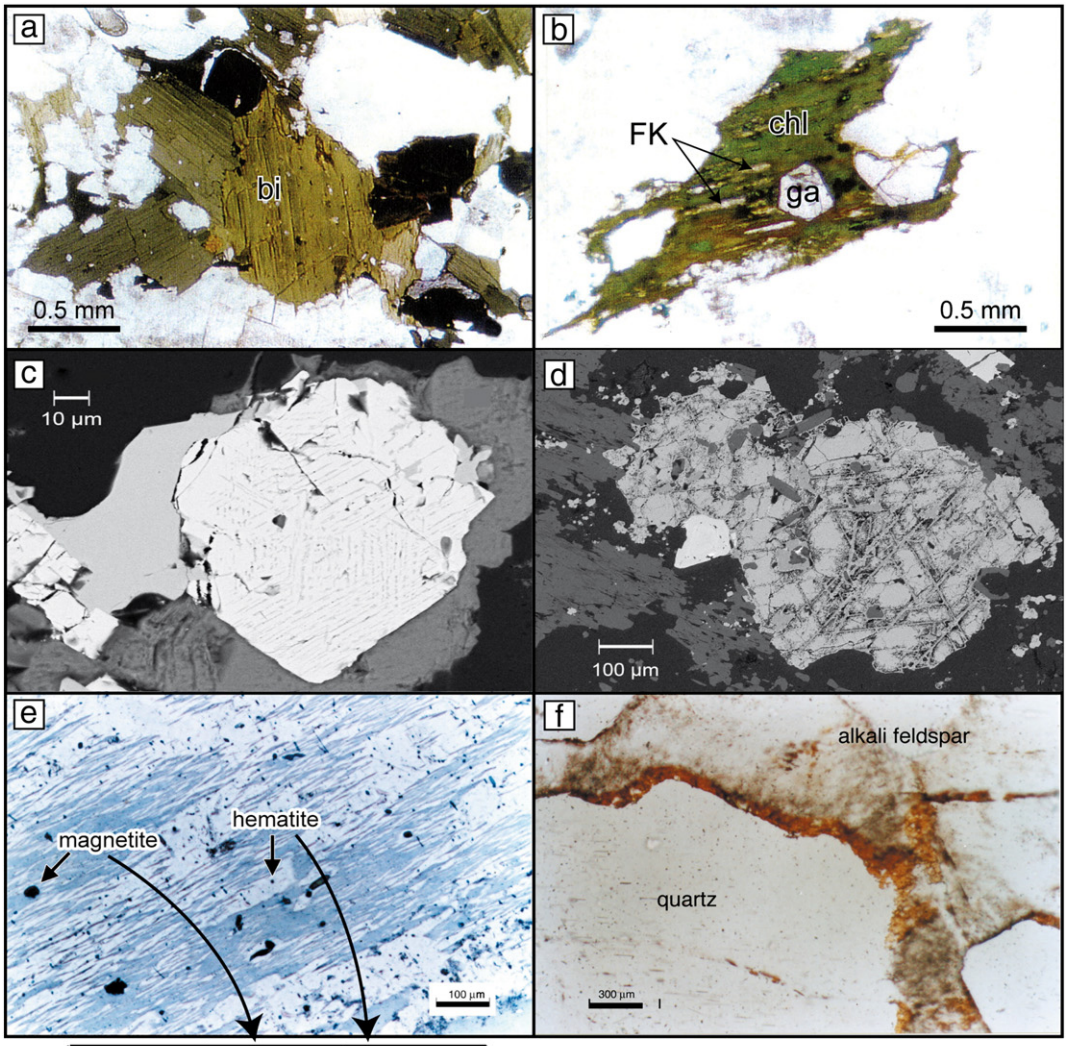

g

	Magnetite (50 µm)	Hematite (10 µm)
SiO_2 (wt %)	0.11	0.29
TiO_2	6.20	5.80
Al_2O_3	0.24	0.19
Fe_2O_3(c)	56.69	93.47
FeO	36.23	-
MnO	0.84	0.69
Sum	100.32	100.43
Si	0.00	0.01
Ti	0.18	0.11
Al	0.01	0.01
Fe^{3+}	1.63	1.82
Fe^{2+}	1.16	-
Mn^{2+}	0.03	0.02
Sum Cations	3.00	1.97

h

Fig. 10. Microphotographs: (a) biotite (bi) and large magnetite grain in unaltered Tana granite; (b) chloritized biotite (chl) with lenses of secondary alkali feldspar (FK) and Ti-oxides in an altered Tana specimen; Ga: garnet; (c) large primary magnetite with ilmenite exsolutions in Meruoca; (d) altered and partly resorbed magnetite with unmodified ilmenite exsolutions in Meruoca; and (e, f, g) detail of Wachita 1 perthitic alkali feldspar with compositions of iron oxide inclusions and microphotograph of Wachita 2 sample with iron hydroxide coatings at the quartz–feldspar boundary; (h) SEM observations of altered Tana granite with secondary (left) and back-scattered (right) electrons: hydrothermal hematite crystals in a vug or dissolution pocket inside an alkali feldspar grain; scale bar: 3 µm.

References

Anderson, J.L., Morrison, J., 2005. Ilmenite, magnetite and peraluminous mesoproterozoic anorogenic granites of Laurentia and Baltica. Lithos 80, 45–60.

Archanjo, C.J., Launeau, P., Hollanda, M.H.B.M., Macedo, J.W., Liu, D., 2009. Scattering of magnetic fabrics in the Cambrian alkaline granite of Meruoca (Ceará state, northeastern Brazil). International Journal of Earth Sciences 98, 1793–1807.

Bailey, S.W., 1984. Structures of layer silicates. In: Brindley, G.W., Brown, G. (Eds.), Structures of clay minerals and their X-ray identification. Mineral Society, London, pp. 1–124.

Bonin, B., 1980. Les complexes alcalins continentaux: l'exemple de la Corse. (Ph. D. thesis), Univ. Paris VI (388 pp.).

Bonin, B., 1986. Ring complex granites and anorogenic magmatism. Studies in GeologyNorth Oxford Academic (188 pp.).

Bonin, B., Platevoet, B., Vialette, Y., 1987. The geodynamic significance of alkaline magmatism in the Western Mediterranean compared with West Africa. In:

Bowden, P., Kinnaird, J.A. (Eds.), African Geology Reviews. Geol. J. (Thematic Issue), pp. 361–387.
Bouchez, J.L., 2000. Anisotropie de susceptibilité magnétique et fabrique des granites. Comptes Rendus. Comptes Rendus. Académie des Sciences (Paris) 330, 1–14.
Burnham, C.W., 1979. Magmas and hydrothermal fluids. Geochemistry of hydrothermal ore deposits 2, 71–136.
Cocherie, A., Rossi, P., Fanning, C.M., Guerrot, C., 2005. Comparative use of TIMS and SHRIMP for U–Pb zircon dating of A-type granites and mafic tholeiitic layered complexes and dykes from the Corsican Batholith (France). Lithos 82, 185–219.
Day, R., Fuller, M., Schmidt, V.A., 1977. Hysteresis properties of titanomagnetites: grain size and compositional dependence. Earth and Planetary Science Letters 13, 260–267.
Daly, R.A., 1928. Bushveld igneous complex of the Transvaal. Geological Society of America Bulletin 39, 703–768.
Dearing, J.A., Dann, R.J.L., Hay, K., Lees, J.A., Loveland, P.J., Maher, B.A., O'Grady, K., 1996. Frequency-dependent susceptibility measurements of environmental materials. Geophysical Journal International 124, 228–240.
Dideriksen, K., Christiansen, B.C., Frandsen, C., Balic-Zunic, T., Mørup, S., Stipp, S.L.S., 2010. Paleo-redox boundaries in fractured granite. Geochimica et Cosmochimica Acta 74, 2866–2880.
Dauphas, N., Roskosz, M., Alp, E.E., Neuville, D.R., Hu, M.Y., Sio, C.K., Tissot, F.L.H., Zhao, J., Tisssandier, L., Médard, E., Cordier, C., 2014. Magma redox and structural controls on iron isotope variations in Earth's mantle and crust. Earth and Planetary Science Letters 398, 127–140.
Dunlop, D.J., 2002. Theory and application of the Day plot (Mrs/Ms versus Hcr/Hc) - 1. Theoretical curves and tests using titanomagnetite data. Journal of Geophysical Research 107. http://dx.doi.org/10.1029/2001JB000486.
Ferré, E., Wilson, J., Gleizes, G., 1999. Magnetic susceptibility and AMS of the Bushveld alkaline granites, South Africa. Tectonophysics 307, 113–133.
Font, E., Trindade, R.I.F., Nédélec, A., 2006. Remagnetization in bituminous limestones of the Neoproterozoic Araras Group (Amazon Craton): hydrocarbon maturation, burial diagenesis or both? Journal of Geophysical Research 111, B06204. http://dx.doi.org/10.1029/2005JB004106.
Gilbert, M.C., 1983. Timing and chemistry of igneous events associated with the southern Oklahoma aulacogen. Tectonophysics 94, 439–455.
Grégoire, V., Darrozes, J., Gaillot, P., Nédélec, A., Launeau, P., 1998. Magnetite grain shape fabric and distribution anisotropy versus rock magnetic fabric: a 3D-case study. Journal of Structural Geology 20, 937–944.
Harding, K.L., Morris, W.A., Balch, S.J., Lapointe, P., Latham, A.G., 1988. A comparison of magnetic character and alteration in three granite drill cores from eastern Canada. Canadian Journal of Earth Sciences 25, 1141–1150.
Heimann, A., Beard, B.L., Johnson, C.M., 2008. The role of volatile exsolution and subsolidus fluid/rock interactions in producing high Fe-56/Fe-54 ratios in siliceous igneous rocks. Geochimica et Cosmochimica Acta 72, 4379–4396.
Hofmeister, A.M., Rossman, G.R., 1983. Color in feldspars, In: Ribbe, P.H. (Ed.), Feldpsar Mineralogy, 2nd edition. Reviews in Mineralogy 2, pp. 271–280.
Hogan, P., Gilbert, M.C., 1995. The A-type Mount Scott granite sheet: importance of crustal magma traps. Journal of Geophysical Research 100 (15,779–15,772).
Hogan, J.P., Gilbert, M.C., Weaver, B.L., Myers, J.D., 1992. High level A-type sheet granites of the Wichita Mountains Igneous Province, Oklahoma, USA. In: Brown, P.E., Chappell, B.W. (Eds.), In Second Hutton Symposium: The Origin of Granites and Related Rocks. Trans. R. Soc. Edinburgh 83, pp. 491–492.
Huang, F., Chakraborty, P., Lundstrom, C.C., Holmden, C., Glessner, J.J.G., Kieffer, S.W., Lesher, C.E., 2010. Isotope fractionation in silicate melts by thermal diffusion. Nature 464, 396–400.
Jackson, M., Gruber, W., Marvin, J., Banerjee, S.K., 1988. Partial anhysteretic remanence and its anisotropy: applications and grainsize-dependence. Geophysical Research Letters 15, 440–443.
Jackson, M., Rochette, P., Fillon, G., Banerjee, S., Marvin, J., 1993. Rock magnetism of remagnetized Paleozoic carbonates: low-temperature behavior and susceptibility characteristics. Journal of Geophysical Research 98, 6217–6225.
Jelinek, V., 1981. Characterization of the magnetic fabric of rock. Tectonophysics 79, 63–67.
Just, J., Kontny, A., De Wall, H., Hirt, A.M., Martín-Hernández, F., 2004. Development of magnetic fabrics during hydrothermal alteration in the Soultz-sous-Forêts granite from the EPS-1 borehole, Upper Rhine graben. In: Martín-Hernández, F., Lüneburg, C.M., Aubourg, C., Jackson, M. (Eds.), Magnetic Fabric: Methods and Applications. Geological Society of London Special Publication 238, pp. 500–526.
Kleemann, G.J., Twist, D., 1989. The compositionally-zoned sheet-like granite pluton of the Bushveld complex: evidence bearing on the nature of A-type magmatism. Journal of Petrology 30, 1383–1414.
Kruiver, P.P., Dekkers, M.J., Heslop, D., 2001. Quantification of magnetic coercivity components by the analysis of acquisition curves of isothermal remanent magnetisation. Earth and Planetary Science Letters 189, 269–276.
Lapointe, P., Morris, W.A., Harding, K.L., 1986. Interpretation of magnetic susceptibility: a new approach to geophysical evaluation of the degree of rock alteration. Canadian Journal of Earth Sciences 23, 393–401.
Lowrie, W., 1990. Identification of ferromagnetic minerals in a rock by coercivity and unblocking temperature properties. Geophysical Research Letters 17, 159–162.
Lundstrom, C., 2009. Hypothesis for the origin of convergent margin granitoids and Earth's continental crust by thermal migration zone refining. Geochimica et Cosmochimica Acta 73, 5709–5729.
Maher, B.A., 1988. Magnetic properties of some synthetic sub-micron magnetites. Geophysical Journal International 94, 83–96.
Marks, M., Vennemann, T., Siebel, W., Markl, G., 2003. Quantification of magmatic and hydrothermal processes in a peralkaline syenite–alkali granite complex based on textures, phase equilibria and stable and radiogenic isotopes. Journal of Petrology 44, 1247–1280.
Nédélec, A., Paquette, J.L., Bouchez, J.L., Olivier, P., Ralison, B., 1994. Stratoid granites of Madagascar: structure and position in the Panafrican orogeny. Geodinamica Acta 7, 48–56.
Nédélec, A., Stephens, W.E., Fallick, A.E., 1995. The Panafrican stratoid granites of Madagascar: alkaline magmatism in a post-collisional extensional setting. Journal of Petrology 36, 1367–1391.
Paquette, J.L., Nédélec, A., 1998. A new insight into Panafrican tectonics in the East–West Gondwana collision zone by U–Pb zircon dating of granites from central Madagascar. Earth and Planetary Science Letters 155, 45–56.
Poitrasson, F., Freydier, R., 2005. Heavy iron isotope composition of granites determined by high resolution MC–ICP-MS. Chemical Geology 222, 132–147.
Poitrasson, F., Pin, C., Duthou, J.L., Platevoet, B., 1994. Aluminous subsolvus anorogenic granite genesis in the light of Nd isotopic heterogeneity. Chemical Geology 112, 199–219.
Poitrasson, F., Paquette, J.L., Montel, J.M., Pin, C., Duthou, J.L., 1998. Importance of late-magmatic and hydrothermal fluids on the Sm–Nd isotope mineral systematics of hypersolvus granites. Chemical Geology 146, 187–203.
Poitrasson, F., Chenery, S., Shepherd, T.J., 2000. Electron microprobe and LA–ICP-MS study of monazite hydrothermal alteration: implications for U–Th–Pb geochronology and nuclear ceramics. Geochimica et Cosmochimica Acta 64, 3283–3297.
Price, J., Hogan, J.P., Gilbert, M.C., Payne, J.D., 1998. Surface and near-surface investigation of the alteration of the Mount Scott granite and geometry of the Sandy Creek gabbro pluton, Hale Spring area, Wichita mountains, Oklahoma. In: Hogan, J.P., Gilbert, M.C. (Eds.), Central North America and Other Regions 12. Kluwer Academic Publisher, Basement Tectonics, pp. 79–122.
Putnis, A., Hinrichs, R., Putnis, C.V., Golla-Schindler, U., Collins, L.G., 2007. Hematite in porous red-clouded feldspars: evidence of large-scale crustal fluid–rock interactions. Lithos 95, 10–18.
Riller, U., Cruden, A.R., Schwerdtner, W.M., 1996. Magnetic fabric and microstructural evidence for a tectono-thermal overprint of the early Proterozoic Murray pluton, central Ontario, Canada. Journal of Structural Geology 18, 1005–1016.
Robb, L.J., Freeman, L.A., Armstrong, R.A., 2000. Nature and longevity of hydrothermal fluid flow and mineralisation in granites of the Bushveld Complex, South Africa. Transactions of the Royal Society of Edinburgh: Earth Sciences 91, 269–281.
Rochette, P., Jackson, M., Aubourg, C., 1992. Rock magnetism and the interpretation of anisotropy of magnetic susceptibility. Reviews of Geophysics 30, 209–226.
Rye, R.O., 1993. The evolution of magmatic fluids in the epithermal environment: the stable isotope perspective. Economic Geology 88, 733–753.
Santos, T.J.S., Fetter, A., Hackspacher, P.C., Van Schmus, W.R., Nogueira Neto, J.A., 2008. Neoproterozoic tectonic and magmatic episodes in the NW sector of Borborema Province, NE Brazil, during assembly of Western Gondwana. Journal of South American Earth Sciences 25, 271–284.
Saunier, G., Poitrasson, F., Moine, B.N., Grégoire, M., Seddiki, A., 2010. Effect of hot desert weathering on the bulk-iron isotope composition of L6 and H5 ordinary chondrites. Meteoritics and Planetary Science 45, 195–209.
Schoenberg, R., von Blanckenburg, F., 2006. Modes of planetary-scale Fe isotope fractionation. Earth and Planetary Science Letters 252, 342–359.
Schuessler, J., Schoenberg, R., Sigmarsson, O., 2009. Iron and lithium isotope systematics of the Hekla volcano, Iceland — evidence for Fe isotope fractionation during magma differentiation. Chemical Geology 258, 78–91.
Sheppard, S.M.F., 1986. Igneous rocks: III. Isotopic case studies of magmatism in Africa, Eurasia and oceanic islands. In: Valley, J., Taylor, H.P., O'Neil, J.R. (Eds.), Stable Isotopes in High Temperature Geological Processes. Reviews in Mineralogy 16, pp. 319–371.
Sial, A.N., Long, L.E., 1987. Mineral chemistry and stable isotope geochemistry of the Meruoca and Mucambo plutons, Ceará, northeast Brazil. International Symposium on Granites and Associated Mineralizations (ISGAM), Salvador, Brazil, pp. 185–188.
Sial, A.N., Figueiredo, M.C.H., Long, L.E., 1981. Rare-earth element geochemistry of the Meruoca and Mucambo plutons, Ceará, northeast Brazil. Chemical Geology 31, 271–283.
Sossi, P.A., Foden, J.D., Halverson, G.P., 2012. Redox-controlled iron isotope fractionation during magmatic differentiation: an example from the Red Hill intrusion, S. Tasmania. Contributions to Mineralogy and Petrology 164, 757–772.
Taylor, H.P., 1978. Oxygen and hydrogen isotope studies of plutonic granitic rocks. Earth and Planetary Science Letters 38, 177–210.
Telus, M., Dauphas, N., Moynier, F., Tissot, F.L.H., Teng, F.Z., Nabelek, P.I., Craddock, P.R., Groat, L.A., 2012. Iron, zinc, magnesium and uranium isotopic fractionation during continental crust differentiation: the tale from migmatites, granitoids, and pegmatites. Geochimica et Cosmochimica Acta 97, 247–265.
Trindade, R.I.F., Bouchez, J.L., Bolle, O., Nédélec, A., Peschler, A., Poitrasson, F., 2001. Secondary fabrics revealed by remanence anisotropy: methodological study and examples from plutonic rocks. Geophysical Journal International 147, 310–318.
Walraven, F., Hattingh, E., 1993. Geochronology of the Nebo granite, Bushveld Complex. South African Journal of Geology 96, 31–41.
Wenner, D.B., Taylor, H.P., 1976. Oxygen and hydrogen isotope studies of a Precambrian granite–rhyolite terrane, St François Mountains, Missouri. Geological Society of America Bulletin 87, 1587–1598.
Whalen, J.B., Currie, K.L., Chappell, B.W., 1987. A-type granites: geochemical characteristics, discrimination and petrogenesis. Contributions to Mineralogy and Petrology 87, 319–327.
Wiederhold, J.G., Teutsch, N., Kraemer, S.M., Halliday, A.N., Kretzchmar, R., 2007. Iron isotope fractionation in oxic soils by mineral weathering and podzolization. Geochimica et Cosmochimica Acta 7, 5821–5833.
Zák, J., Schulmann, K., Hrouda, F., 2005. Multiple magmatic fabrics in the Sazáva pluton (Bohemian Massif, Czech Republic): a result of superposition of wrench-dominated regional transpression on final emplacement. Journal of Structural Geology 27, 805–822.